Deletion of a Highly Motional Residue Affects Formation of the Michaelis Complex for *Escherichia coli* Dihydrofolate Reductase†

Grover Paul Miller‡ and Stephen J. Benkovic*

Department of Chemistry, The Pennsylvania State University, University Park, Pennsylvania 16802

Received December 1, 1997; Revised Manuscript Received March 6, 1998

ABSTRACT: Analysis of the dihydrofolate reductase (DHFR) complex with folate by two-dimensional heteronuclear ($^1H-^{15}N$) nuclear magnetic relaxation revealed that isolated residues exhibit diverse backbone fluctuations on the nanosecond to picosecond time scale [Epstein, D. M., Benkovic, S. J., and Wright, P. E. (1995) *Biochemistry 34,* 11037−11048]. These dynamical features may be significant in forming the Michaelis complex. Of these residues, glycine 121 displays large-amplitude backbone motions on the nanosecond time scale. This amino acid, strictly conserved for prokaryotic DHFRs, is located at the center of the βF−βG loop. To investigate the catalytic importance of this residue, we report the effects of Gly121 deletion and glycine insertion into the modified βF−βG loop. Relative to wild type, deletion of Gly121 dramatically decreases the rate of hydride transfer 550-fold and the strength of cofactor binding 20-fold for NADPH and 7-fold for $NADP^+$. Furthermore, ΔG121 DHFR requires conformational changes dependent on the initial binary complex to attain the Michaelis complex poised for hydride transfer. Surprisingly, the insertion mutants displayed a significant decrease in both substrate and cofactor binding. The introduction of glycine into the modified βF−βG loop, however, generally eliminated conformational changes required by ΔG121 DHFR to attain the Michaelis complex. Taken together, these results suggest that the catalytic role for the βF−βG loop includes formation of liganded complexes and proper orientation of substrate and cofactor. Through a transient interaction with the Met20 loop, alterations of the βF−βG loop can orchestrate proximal and distal effects on binding and catalysis that implicate a variety of enzyme conformations participating in the catalytic cycle.

Dihydrofolate reductase (5,6,7,8-tetrahydrofolate:$NADP^+$ oxidoreductase, EC 1.5.1.3; DHFR)[1] utilizes NADPH to reduce 7,8-dihydrofolate (H_2F) to 5,6,7,8,-tetrahydrofolate (H_4F). Maintenance of the intracellular pool of H_4F is critical for the biosynthesis of purines, pyrimidines, and several amino acids (*1*), such as thymidylate, a building block of DNA. Consequently, the enzyme has been a long-standing target for inhibiting DNA synthesis in cancer cells (*2*) and in bacteria (*3*).

Due to the wealth of crystallographic (ref *4* and references therein) and solution structure information (*5*−*7*) and of kinetic (*8*) and computational analyses (*9*), DHFR is an ideal candidate for studying elements of catalysis. For example, enzymes are known to display dynamical fluctuations on various time scales; nevertheless, demonstrating how these dynamics contribute to catalysis is difficult. A hallmark of NMR studies is the description of protein dynamics. Studies employing NMR techniques have probed the solution structure of DHFR in the absence and presence of ligands (*5*−*7*). Analysis of the two-dimensional nuclear Overhauser spectra of the apoenzyme suggests the Met20 loop exists in an equilibrium between two conformations (*6*). As an indicator of Met20 loop dynamics, the exchange of Trp22 between two environments (35 s^{-1}) is similar to the off rates of ligands. The relaxation characteristics of the DHFR·folate complex provides further insight into backbone and tryptophan side-chain dynamics using uniformly ^{15}N-labeled DHFR (*7*). Six sites exhibit large backbone motional amplitudes on the nanosecond to picosecond time scale that serve to distinguish these regions from the lower amplitude backbone fluctuations associated with the rest of the enzyme. The location of these residues in loop regions indicates the retention of high flexibility for these regions in the binary folate complex. A functional role for the observed flexibility in all regions is not apparent.

Of these highly motional residues, Gly121 is located at the center of the βF−βG loop (residues 117−131) about 19 Å from the active-site aspartate, or 8 Å from bound cofactor, as shown in Figure 1 (*4*). High B-factors in X-ray crystal structures indicate that the βF−βG loop is quite flexible in

† This work was supported in part by NIH Grant GM24129.

* To whom the correspondence should be addressed: Tel 814-865-2882; Fax 814-865-2973; email sjb1@psu.edu.

‡ Recipient of Homer F. Braddock College of Science Memorial Scholarship.

[1] Abbreviations: DHFR, dihydrofolate reductase; ΔG121 DHFR, *Escherichia coli* dihydrofolate reductase, mutant in which glycine 121 has been deleted; 117.5G,ΔG121 DHFR, insertion of glycine between alanine 117 and glutamate 118 in ΔG121 dihydrofolate reductase, preserving original wild-type numbering of amino acids; ΔG121,124.5G DHFR, insertion of glycine between histidine 124 and phenylalanine 125 in ΔG121 dihydrofolate reductase, preserving original wild-type numbering of amino acids; MTX, methotrexate; H_2F, 7,8-dihydrofolate; H_4F, 5,6,7,8-tetrahydrofolate; NADPH or NH, nicotinamide adenine dinucleotide phosphate, reduced; NADPD, [(4′*R*)-^{2}H]nitocintamide adenine dinucleotide phosphate, reduced; DNADPH, 5,6-dihydronitocintamide adenine dinucleotide phosphate, reduced; $NADP^+$ or N^+, nicotinamide adenine dinucleotide phosphate, oxidized; EDTA, ethylenediaminetetraacetic acid; DTT, dithiothreitol.

S0006-2960(97)02922-X CCC: $15.00
Published on Web 04/16/1998

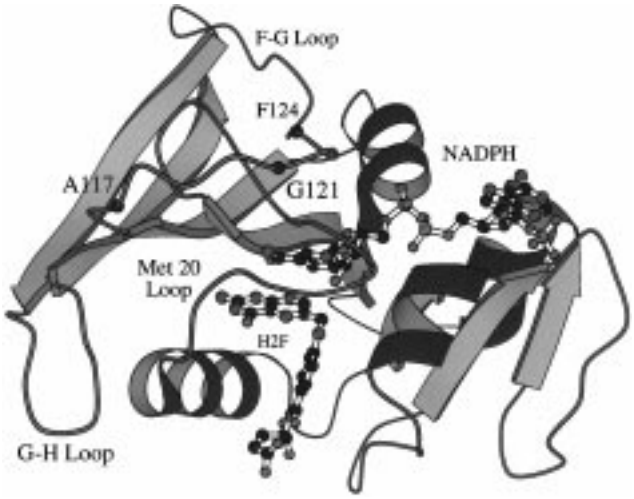

FIGURE 1: Model of the reactive DHFR·NADPH·H_2F complex. The figure illustrates the relative positions of the substrate and cofactor to the relevant protein elements (the βF−βG loop, Gly121, and points of glycine insertion, Ala117 and Phe124). The X-ray crystal structure of the DHFR·$NADP^+$·folate complex (*1*) was used to construct this figure using MOLSCRIPT.

the absence of bound ligand; however, the binding of ligand introduces order into the βF−βG and Met20 loops, where the outer βF−βG loop actually folds over the Met20 loop (*10*). Conservation of Gly121 among prokaryotes suggests a common function may exist for this flexible residue.

A structural role for Gly121 has been investigated by saturation mutagenesis (*11, 12*), which demonstrated that increased side-chain hydrophobicity decreased DHFR stability to temperature and denaturants. The same mutants exhibited effects on catalysis under steady-state conditions, thereby linking the structural role of glycine 121 to catalysis. Although the identity of the affected steps within the catalytic cycle was not determined, mutant DHFRs showed decreased k_{cat}/K_m values relative to wild type, stemming from a lower rate of turnover (k_{cat}) than binding of substrate (K_m). Changes in catalysis were attributed to a loss in flexibility at the 121 position.

Further analysis of G121V DHFR by our laboratory indicated that this mutation drastically reduces cofactor binding and catalysis (*13*). Interestingly, the steady-state rate contains contributions from the rate of hydride transfer (1.3 s^{-1}) and a novel conformational change (3.5 s^{-1}) ascribed to an isomerization of the initial ternary complex, DHFR·NADPH·H_2F, to one poised for catalysis. In the absence of structural data, it is not possible to accurately described the nature of the conformational change; however, the introduction of a conformational change is indicative of the dynamical property of Gly121, as suggested in the NMR analysis of the DHFR·folate complex (*7*).

As a complement to this work, we constructed and characterized kinetically mutant DHFRs containing modified βF−βG loops. To address the role of motional freedom at Gly121, this residue was deleted to yield ΔG121 DHFR. The construction of a partial kinetic scheme for ΔG121 DHFR demonstrates a more severe effect of this mutation on the catalytic cycle than the G121V substitution. Notably, this mutation compromises the pathway to attain the Michaelis complex. Since deletion of Gly121 shortens the βF−βG loop, an attempt was made to reconstitute the length of this loop by reinsertion of glycine into the ΔG121 βF−βG loop. Specifically, glycine was inserted at either of two positions at the base of the ΔG121 βF−βG loop, between A117 and E118 (117.5G,ΔG121 DHFR) or between H124 and F125 (ΔG121,124.5G DHFR). The insertion mutants were characterized by determining the binding of substrate and cofactor, the rate of the hydride transfer, and the presence or absence of conformational changes, as observed with ΔG121 DHFR. The effects of these mutations underscore the critical relationship of interloop contacts to guide complex formation and further implicate a dynamic quality to these interactions.

MATERIALS AND METHODS

Mutagenesis

Materials. Standard DNA procedures were followed as described (*14*). Propagation of plasmid DNA was carried out using *Escherichia coli* DH5α cells. Restriction and DNA modifying enzymes were purchased from New England Biolabs or Promega. Oligonucleotides for mutagenesis were synthesized on a 8909 Perceptive Biosystems DNA synthesizer. Sequencing of plasmid DNA was performed by the Nucleic Acids Facility at the Pennsylvania State University.

Construction of DHFR Mutants. The introduction of the desired mutations was performed using the overlap extension technique (*15*). The expression plasmid pET22b-DHFR-ΔG121 (provided courteously by C. E. Cameron) was used as a template for the first polymerase chain reaction (PCR). Relevant primers are listed in Table 1. In brief, two independent PCR reactions were conducted: one reaction with the DHFR-For and the mutagenic reverse primers, and the other reaction with the mutagenic forward and DHFR-Rev primers. The resulting products were gel purified and then used in a subsequent amplification employing the DHFR-For and DHFR-Rev primers. The desired expression construct was obtained by restriction digest of the mutant gene with *Cla*I and *Bam*HI and then ligation into the pET22b-DHFR vector. The presence of the mutations was confirmed by sequencing.

Protein Purification

Materials. The BL21(DE3) strain of *E. coli* was used for expression of DHFR proteins using a pET22b-derived plasmid (Novagen) and induced by isopropyl β-D-thiogalactoside (IPTG). The purification of DHFR utilized the following buffers: lysis buffer (25 mM sodium phosphate, pH 7.0, 5 mM EDTA, and 10% glycerol), PEG buffer (25 mM sodium phosphate, pH 7.0, 500 mM NaCl, 18% PEG 8000, and 10% glycerol), Buffer A (25 mM sodium phosphate, pH 7.0, 500 mM NaCl, 1 mM DTT, and 10% glycerol); buffer B (100 mM boric acid, pH 9.3, 500 mM NaCl, 5 mM folic acid, 1 mM DTT, and 10% glycerol), buffer C (50 mM Tris-HCl, pH 7.5, 1.0 mM DTT, and 10% glycerol), and storage buffer (50 mM sodium phosphate, pH 7.0, 1 mM DTT, and 10% glycerol). These reagents were obtained from Fisher Scientific and Sigma Chemical Co. Methotrexate−agarose was purchased from Sigma Chemical Co. All concentrations are final concentrations.

Affinity Purification. The production of dihydrofolate reductase (DHFR) utilized the *E. coli* strain BL21(DE3) cells

Table 1: Primers for Site-Directed Mutagenesis of the DHFR Gene

primer	nucleotide sequence
DHFR-For	5′GCG GGA TCC CAT ATG ATC AGT CTG ATT GCG GCG3′
DHFR-117.5G,ΔG121-For	5′ACG CAT ATC GAT GCA GGC GAA GTG GAA3′
DHFR-ΔG121,124.5G-For	5′GAC ACC CAT GGC TTT CCG GAT TAC3′
DHFR−Rev	5′GCG TCT AGA GGA TCC TTA ACG ACG CTC GAG GAT3′
DHFR-117.5G,ΔG121-Rev	5′TTC CAC TTC GCC TGC ATC GAT ATG CGT3′
DHFR-ΔG121,124.5G-Rev	5′GTA ATC CGG AAA GCC ATG GGT GTC3′

transformed with the pET-22b-derived expression plasmid. Cells containing the pET22b-derived expression were grown at 37 °C to OD_{600} 0.8 in NCZYM medium (Gibco-BRL) containing 200 μg mL^{-1} ampicillin and induced with 0.4 mM IPTG. After a 4 h induction at 37 °C, the cells were harvested by centrifugation at 4 °C. The resulting 3 g L^{-1} wet cell pellet was resuspended in 12.5 mL of lysis buffer and lysed with the addition of 1 mg mL^{-1} lysozyme. At 4 °C the following were added to the lysed cell solution: 175 μL of 1.0 M DTT, 500 μL of 100 mM phenylmethanesulfonyl fluoride, 100 μL of 1.4 mg mL^{-1} pepstatin, 100 μL of 1 mg mL^{-1} leupeptin, 850 μL of 5 M NaCl, and 850 μL of 25% Triton X-100. After 15 min of stirring, 1.5 mL of 5 M NaCl was added, followed by 11.5 mL of PEG buffer (added slowly). After 60 min of stirring, the mixture was ultracentrifuged (70 Ti rotor at 30 000 rpm, 30 min, 4 °C).

The crude lysate was dialyzed against buffer A and loaded on a 5 mL methotrexate−agarose column previously equilibrated with buffer A. Elution of DHFR from this column was accomplished with buffer B, collecting about 12 fractions (1.5 mL each). Fractions were analyzed by SDS−PAGE, and samples containing DHFR were pooled. Folate was removed by dialysis against buffer C, and then the sample was loaded on a 12 mL Whatman DE-52 (1.5 cm i.d.) column. Elution of DHFR was performed using a salt gradient from 0 mM NaCl (45 mL) to 500 mM NaCl (50 mL) in buffer C. Fractions from the column were 3 mL. DHFR was eluted around 300 mM NaCl as determined by absorbance at 280 nm. The appropriate fractions were pooled and dialyzed against storage buffer before final storage at 4 °C. DHFR was quantitated either spectrophotometrically (ϵ_{280} = 0.0746 μM^{-1} cm^{-1}) or by active-site titration with MTX (*16*). Values obtained by these methods were within 10%. A typical preparation from 1 L of cells yielded about 5 mg of protein.

Preparation of DHFR Ligands

Materials. A common buffer employed in the purification of ligands was triethylammonium bicarbonate (TEAB). A 1 M stock was made by bubbling CO_2 through a 1 M solution of triethylamine (Aldrich) in an ice bath until pH 7.5 and then storing at 4 °C. Purchased from Sigma, Aldrich, or Acros were folate, methotrexate, $NADP^+$, NADPH, sodium hydrosulfite (88% pure dithionite), Pd−C (10%), β-mercaptoethanol, 2-propanol-d_8 (> 99% D), and *Thermoanaerobium brocki* aldehyde dehydrogenase.

Cofactor Derivatives. The cofactor, [4′(*R*)-^{2}H]NADPH (NADPD), was made as described (*17*) and purified on a 10 mL Whatman DE-52 (1.5 cm i.d.) column. The cofactor was eluted using a linear gradient from 4 mM (45 mL) to 700 mM (50 mL) TEAB. The cofactor was found at 500 mM TEAB as determined by absorbance at 340 nm. Synthesis of 5,6-dihydro-NADPH (DNADPH) was accomplished by reduction of NADPH under 1 atm of hydrogen by a palladium−carbon catalyst (*18*). The resulting compound was purified as described for NADPD except elution of cofactor was detected using absorbance at 260 nm. The concentrations of ligand solutions were determined spectrophotometrically [NADPH(D), ϵ_{340} = 6.22 mM^{-1} cm^{-1}; $NADP^+$ and DNADPH, ϵ_{260} = 18 mM^{-1} cm^{-1} (absorbance of adenine ring)].

Folyl Compounds. The substrate, dihydrofolate (H_2F), was prepared from folic acid by dithionite reduction (*19*), whereas the product, (6*S*)-tetrahydrofolate (H_4F), was prepared from H_2F by using *E. coli* dihydrofolate reductase (*20*). The folyl product was purified from the crude reaction using a Whatman DE-52 column (80 mL of resin in 2.5 cm i.d. column) with a linear gradient from 200 mM (350 mL) to 700 mM TEAB (375 mL). Tetrahydrofolate was detected by following absorbance at 297 nm (*21*). The concentrations of ligand solutions were determined spectrophotometrically (H_2F, ϵ_{282} = 28 mM^{-1} cm^{-1}; H_4F, ϵ_{297} = 28 mM^{-1} cm^{-1}; MTX, ϵ_{302} = 22.1 mM^{-1} cm^{-1}).

Characterization of Wild-Type and Mutant DHFRs

Materials. All assays were conducted using the buffer MTEN [50 mM MES [2-(*N*-morpholino)ethanesulfonic acid], 25 mM Tris [tris(hydroxymethyl)aminomethane], 25 mM ethanolamine, and 100 mM NaCl] at 25 °C. The pH of this buffer was adjusted to pH 7.0 or 9.0, depending on the design of the experiment. The components of this buffer were obtained from Fisher Scientific.

Equilibrium Dissociation Constants. The dissociation constant, K_D, was measured by ligand quenching of intrinsic protein fluorescence as a function of ligand concentration using an SLM Aminco 8000 spectrofluorometer (SLM Aminco Instruments, Inc.). Typically, DHFR was added to filtered, degassed MTEN buffer at pH 7.0 in a fluorescence cuvette. Tryptophan fluorescence was monitored at 340 nm from excitation at 290 nm. The addition of ligand resulted in a fluorescence decrease. After correction for inner filter effects, the data were fit to a quadratic equation (*22*). Acceptable K_D determinations were made using concentrations of enzyme below the respective K_D value. To quantitate DHFR, the active site was titrated with MTX using fluorescence quenching as stated above. If the protein concentration exceeds the K_D value for the ligand by 10-fold, a monotonic decrease in fluorescence will be observed until the site is saturated. A fit of these data yields the concentration of active DHFR. All binding studies were performed at pH 7.0.

Steady-State Kinetic Parameters. The rate of substrate turnover under saturating amounts of H_2F and NADPH was determined by monitoring the decrease in NADPH absor-

bance at 340 nm ($\epsilon_{340} = 0.0132\ \mu M^{-1}\ cm^{-1}$). For a typical experiment, 50 nM enzyme was preincubated with NADPH, and the reaction was initiated upon addition of H_2F. For comparative purposes, the addition of specific ligands was reversed, and the resulting k_{cat} value was measured. Concentrations of H_2F and NADPH were varied from 50 to 200 μM to ensure reaction conditions were saturating.

To measure the reverse reaction, the same signal corresponding to NADPH was monitored, except under these conditions NADPH is being produced. Due to the high instability of tetrahydrofolate, attempts were made to minimize contact of H_4F with oxygen, light, and temperatures greater than 4 °C. As a precaution, 5 mM DTT was added to all solutions. For a typical experiment, enzyme (0.1 μM) was preincubated with 2 mM $NADP^+$, and the reaction was initiated upon addition of 100 μM H_4F. Ligand concentrations were varied to ensure saturation of enzyme.

Transient Kinetics. Transient binding and pre-steady-state kinetic experiments were performed on a stopped-flow instrument (Applied Photophysics Ltd.). Ligand binding and competition rates were measured by following quenching of intrinsic enzyme fluorescence. Enzyme tryptophans were excited at 290 nm, resulting in fluorescence at 340 nm through a 305 nm output filter. The addition of ligand quenched the fluorescence resulting in the measured signal. Design of these experiments was based on principles discussed elsewhere (*8*, *23*, *24*). Pre-steady-state rates were measured by monitoring coenzyme fluorescence at 450 nm through a 400 nm output filter. This technique relies on excitation of enzyme tryptophans at 290 nm that subsequently emit at 340 nm, the absorbance band for the nicotinamide ring of reduced cofactor. In a typical experiment, 2.5 μM DHFR was preincubated with saturating NADPH (100 μM) in MTEN at pH 7.0, 25 °C. The addition of a saturating amount of H_2F (100 μM) resulted in a rapid single-exponential burst in signal (product formation proportional to enzyme concentration), followed by a slower rate (steady-state turnover of substrate, k_{cat}). The use of NADPD as a cofactor results in an isotope effect on the burst rate, the chemistry step, of 2.8−3.0. Differences in experimental design for the mutants are discussed in detail in the Results and Discussion section.

RESULTS AND DISCUSSION

Enzymes are known to undergo a variety of conformational changes; nevertheless, demonstrating how these dynamics contribute to catalysis is difficult. The existence of diverse backbone dynamics has been demonstrated in the *E. coli* DHFR·folate complex (*7*). To investigate a possible role for these dynamic motions in catalysis, our group has focused on glycine 121 in the βF−βG loop, implicated by T_1 measurements to be a residue whose amide backbone is moving at a picosecond frequency. In this study we observed the effects of glycine deletion followed by glycine reinsertion on either side of the 121 position. The results of these mutations are discussed in terms of delineating the potential catalytic role of G121 motions within the βF−βG loop, as well as the loop itself.

Thermodynamic Binding of Ligands. To determine the equilibrium dissociation constants (K_D) for respective ligands, quenching of intrinsic enzyme fluorescence was monitored as a function of ligand concentration as described in the Materials and Methods section (Table 2). Deletion of Gly121 affects both reduced and oxidized forms of cofactor. The K_D values for this derivative decrease 20-fold for NADPH and 7-fold for $NADP^+$ relative to wild-type values. Affinity for the cofactor analogue, DNADPH, where the 5,6-double bond of NADPH is reduced, decreases 2-fold for both wild-type and ΔG121 DHFRs. Since the difference between NADPH and DNADPH lies in the nicotinamide ring, this trend indicates a loss in the binding contacts that distinguish these forms of the cofactor. The larger effect of this mutation on NADPH binding versus $NADP^+$ binding is consistent with this conclusion. Of the folyl derivatives, only product binding is affected by deletion of Gly121. This mutant displays a 4-fold loss in affinity for tetrahydrofolate.

Table 2: K_D Values of Ligands for Wild-Type and βF−βG Mutant DHFRs

	K_D (μM)			
ligand	wild type[a]	ΔG121	117.5G,ΔG121	ΔG121,124.5G
MTX	<0.01	<0.01	<0.01	<0.01
NADPH	0.33 ± 0.06	6 ± 1	2.4 ± 0.4	2.8 ± 0.4
DNADPH	0.83 ± 0.07	5.5 ± 0.8	ND[b]	ND
H_2F	0.22 ± 0.06	0.26 ± 0.03	3.9 ± 0.4	2.3 ± 0.2
$NADP^+$	22 ± 4	140 ± 20	ND	ND
H_4F	0.10 ± 0.01	0.41 ± 0.07	ND	ND

[a] Taken from Fierke et al. (*8*). [b] ND, not determined.

To assess the ability of a glycine insertion in the ΔG121 βF−βG loop to recovery wild-type binding of ligands, the K_D values for substrate (H_2F) and cofactor (NADPH) were determined. These data indicate a mixed recovery of binding by these mutants (Table 2). Introduction of glycine at either position induces a 2.3-fold recovery of reduced cofactor binding. Unexpectedly, these glycine insertions introduce a significant loss in substrate binding, a 10- or 20-fold effect. The additional loss of folyl binding suggests the insertion of glycine in the ΔG121 βF−βG loop further disrupts the stability of binary complexes.

Kinetic Binding of Ligands. The relaxation method enables the determination of ligand binding kinetics by measuring quenching of enzyme fluorescence as a function of ligand concentration. Typically, two exponentials are observed during formation of binary complexes: a rapid, ligand-dependent phase followed by a ligand-independent phase (*8*, *24*, *25*). The ligand-dependent phase (k_{obs}) increases linearly as a function of ligand concentration. Under pseudo-first-order conditions, this simple association reaction is described by $k_{obs} = k_{on}[L] + k_{off}$, where k_{on} and k_{off} are the association and dissociation rate constants, respectively. The slower, ligand-independent phase has been attributed to the interconversion between enzyme conformers. As shown in Scheme 1, ligand binds rapidly to one of two enzyme conformers (E_1 and E_2) and interconversion between these conformers is slow (*25*).

Scheme 1

$$E_2 \rightleftharpoons E_1 + L_1 \underset{k_{off}}{\overset{k_{on}}{\rightleftharpoons}} E_1 \cdot L_1$$

Attempts to obtain ligand binding kinetics for NADPH and H_2F to ΔG121 apo-DHFR failed. When 4−32 μM NADPH was added to 0.5 μM ΔG121 DHFR, only a single

ligand-independent phase occurring at 0.082 ± 0.004 s^{-1} was observed (data not shown). Similarly, when 1−50 μM H_2F was added to 0.5 μM ΔG121 DHFR, there was no fast phase. Instead, a ligand-independent phase of 0.080 ± 0.006 s^{-1} was measured (data not shown).

The ligand-independent phase reflects a conformational change that occurs prior to ligand binding. In this scenario, the slow conversion of enzyme to a binding species is followed by rapid binding of ligand. Since the first rate limits binding, the observed rate is independent of ligand concentration. This conformational change may reflect the E_1 and E_2 forms of enzyme observed in the wild-type mechanism. In the case of ΔG121 DHFR, the equilibrium is shifted to strongly favor the non-ligand-binding E_2 species, such that the concentration of E_1 in solution is insufficient to yield a measurable amplitude during these ligand binding studies. Since the E_1 and E_2 forms are defined solely by a wild-type binding phenomenon, it is also conceivable that the two apo forms of ΔG121 DHFR are unique to that mutant. These experiments indicate that ΔG121 apo-DHFR is not poised for binding ligands readily. No attempts were made to assay ligand binding for ternary complexes, since resultant amplitudes are typically smaller than those observed for binary complex formation.

Dissociation Rate Constants for Ligands. Despite the complications of the relaxation technique, dissociation rate constants could be obtained for ligands from all ΔG121 DHFR complexes, employing the competition method (*26*). In this technique, a saturated binary complex ($E{\cdot}L_1$) and a large excess of a second ligand (L_2) are combined. The second ligand competes for free enzyme to yield a signal dependent on the difference in fluorescence quenching by the two ligands (Scheme 2). If $k_1[L_1] \ll k_2[L_2] \gg k_{-1}$, then the observed rate (k_{obs}) is the dissociation rate constant for L_1 (k_{-1} or k_{off}). The independence of k_{obs} on ligand concentrations confirms this conclusion.

Scheme 2

$$E{\cdot}L_1 \underset{k_1}{\overset{k_{-1}}{\rightleftharpoons}} E + L_1$$

$$E + L_2 \underset{k_{-2}}{\overset{k_2}{\rightleftharpoons}} E{\cdot}L_2$$

The results of these types of experiments for ΔG121 DHFR are summarized in Table 3. Attempts to measure the respective off rates of $NADP^+$ from the $E{\cdot}NADP^+{\cdot}H_4F$ and $E{\cdot}NADP^+$ complexes did not result in detectable signals; thus a lower limit (>500 s^{-1}) is assigned to this rate. Overall, NADPH, $NADP^+$, and H_4F off rates increase by 2−7-fold, whereas the off rate for H_2F does not change appreciably compared to wild-type rates. The ligand dissociation rates from DHFR complexes are consistent with a more pronounced effect on binding cofactor than folyl derivatives, as demonstrated with the K_D values for ligands.

Steady-State Kinetics: (A) Forward Reaction. The modifications of the βF−βG loop alter the rate-limiting step in DHFR catalysis. Under saturating conditions of substrate and cofactor at pH 7.0, the rate of substrate turnover (k_{cat}) by wild-type DHFR is determined by the off rate of product from the mixed ternary complex, $DHFR{\cdot}NADPH{\cdot}H_4F$ (*8*). This rate (12 s^{-1}) is much slower than the rate of hydride transfer (220 s^{-1}); thus no isotope effect is observed when NADPD is used as a cofactor. In contrast to wild type, hydride transfer by the deletion mutants becomes the rate-limiting step in the steady state, as evidenced by a full isotope effect (Table 4). The rates were obtained by measuring the decrease in NADPH absorbance at 340 nm, when 100 μM H_2F was added to 0.5 μM enzyme preincubated with 100 μM NADPH. A comparison of the mutant k_{cat} values to the wild-type rate of hydride transfer indicates that this step is decreased 550-fold for ΔG121 DHFR. Introduction of glycine into the ΔG121 βF−βG loop fails to yield any recovery of the rate of chemistry. In fact, hydride transfer actually decreases relative to ΔG121 DHFR. Consistent with the K_D data for ligands, the insertion mutants display different properties than either wild-type or ΔG121 DHFR.

Table 3: Ligand k_{off} Values from Wild-Type and ΔG121 DHFR Complexes

ligand	enzyme species	trap	wild type[a] k_{off} (s^{-1})	ΔG121 k_{off} (s^{-1})
NADPH	$E{\cdot}NADPH$	$NADP^+$	3.6 ± 0.5	8.0 ± 0.8
	$E{\cdot}H_4F{\cdot}NADPH$		85 ± 10	175 ± 8
DNADPH	$E{\cdot}H_2F{\cdot}DNADPH$	$NADP^+$	69 ± 1[b]	241 ± 8
$NADP^+$	$E{\cdot}NADP^+$	NADPH	290 ± 20	>500
	$E{\cdot}H_2F{\cdot}NADP^+$		50 ± 10	360 ± 25
	$E{\cdot}H_4F{\cdot}NADP^+$		200 ± 20	>500
H_2F	$E{\cdot}H_2F$	MTX	22 ± 5	20.0 ± 0.5
	$E{\cdot}H_2F{\cdot}DNADPH$		20.0 ± 0.5	19.0 ± 0.6
	$E{\cdot}H_2F{\cdot}NADP^+$		6.6 ± 1	14.4 ± 0.8
H_4F	$E{\cdot}H_4F$	MTX	1.4 ± 0.2	6.2 ± 0.2
	$E{\cdot}H_4F{\cdot}NADPH$		12 ± 2	33 ± 1
	$E{\cdot}H_4F{\cdot}NADP^+$		2.4 ± 0.2	4.4 ± 0.2

[a] Taken from Fierke et al. (*8*). [b] Value obtained in this study at pH 7.0.

(B) Reverse Reaction. An attempt was made to obtain the rate of the reverse reaction by adding 100 μM H_4F to 0.1 μM ΔG121 DHFR preincubated with 2 mM $NADP^+$. The turnover of H_4F to H_2F results in the concomitant reduction of $NADP^+$ to yield an increase in absorbance at 340 nm (NADPH). Even when the enzyme concentration was varied, no change in absorbance was observed; thus an upper limit is assigned to this rate, reflecting the limit of detection for this assay (<0.003 s^{-1}).

Pre-Steady-State Kinetics. As employed in the ligand-binding experiments, stopped-flow fluorescence permits the measurement of rapid phase kinetics. At pH 7.0, the wild-type hydride transfer rate is much greater than the steady-state rate, 220 s^{-1} versus 12 s^{-1}. The rapid rate of hydride transfer can be obtained under pre-steady-state conditions. Unlike the ligand-binding studies, the measured signal derives from the spectral overlap of enzyme fluorescence at 340 nm with the absorbance of the reduced nicotinamide ring for NADPH. The resulting excited cofactor emits at 450 nm. This fluorescence signal decreases as substrate and cofactor turnover. For wild type, the addition of an excess of substrate to a saturated enzyme−NADPH complex results in a burst followed by a steady-state rate. This burst rate is hydride transfer, demonstrating a full isotope effect of 3.0.

Analysis of steady-state turnover by the ΔG121 mutants indicates the rate of hydride transfer is rate-limiting (Table 4). As such, no burst of product formation would be expected under pre-steady-state conditions after a saturated reactive complex is formed. Surprisingly, fluorescent tran-

Table 4: Steady-State Rates for Wild-Type and βF−βG Mutant DHFRs at pH 7.0

parameter	wild type[a]	ΔG121	117.5G,ΔG121	ΔG121,124.5G
k_{cat} (s^{-1}) for NADPH	12.3 ± 0.7	0.43 ± 0.03	0.28 ± 0.03	0.061 ± 0.007
k_{cat} (s^{-1}) for NADPD	10 ± 1	0.15 ± 0.01	0.10 ± 0.01	0.020 ± 0.003
^{D}V	1.1 ± 0.1	2.9 ± 0.2	2.8 ± 0.3	3.0 ± 0.3

[a] Taken from Fierke et al. (*8*).

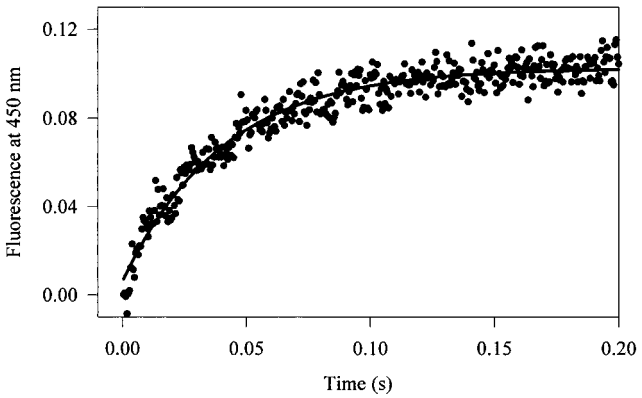

I. E•NADPH ⇌ (fast) E•NADPH•H_2F ⇌ (23 s^{-1}) **E•NADPH•H_2F

II. E•NADPH ⇌ (23 s^{-1}) **E•NADPH ⇌ (fast) **E•NADPH•H_2F

FIGURE 2: Conformational change of ΔG121 mutant DHFR to form the DHFR·NADPH·H_2F complex. The figure describes the fluorescence burst observed upon addition of H_2F to the DHFR·NADPH complex of ΔG121 prior to steady-state turnover. Since the fluorescence transient occurs at a rate much greater than the steady-state rate, only the data for the fluorescence burst are shown and fit to a single exponential. The corresponding rate and error from the fit are discussed in the text. Reactions I and II denote the possible sequence of events resulting in the formation of the reactive complex. Reaction conditions were 3 μM DHFR, 100 μM NADPH, and 100 μM H_2F at 25 °C in MTEN at pH 7.0.

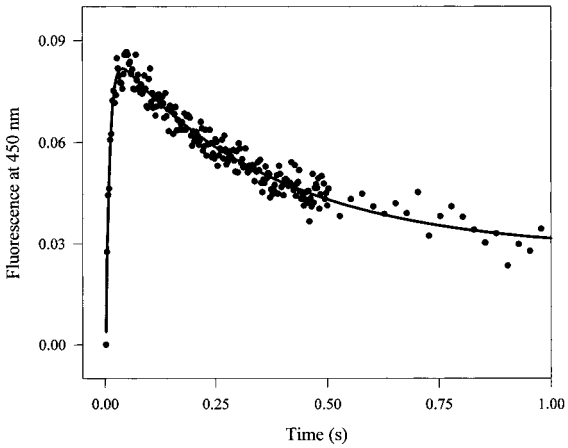

E•H_2F ⇌ (fast) E•NADPH•H_2F ⇌ (112 s^{-1}) *E•NADPH•H_2F ⇌ (5.9 s^{-1}) **E•NADPH•H_2F

FIGURE 3: Conformational change of ΔG121 mutant DHFR to form the DHFR·NADPH·H_2F complex. The figure describes the fluorescence burst, followed by a rapid decrease observed upon addition of NADPH to the DHFR·H_2F complex of ΔG121 prior to steady-state turnover. Since the fluorescence transients occur at a rate much greater than the steady-state rate, only the data for the rapid fluorescence changes are shown and fit to a double exponential. The corresponding rates and error from the fit are discussed in the text. Neither rate was dependent on [NADPH]; thus rates were assigned to conformational changes. The reaction shown denotes the sequence of events resulting in the formation of the reactive complex. Reaction conditions were 3 μM DHFR, 100 μM NADPH, and 100 μM H_2F at 25 °C in MTEN at pH 7.0.

sients are observed by fluorescence resonance energy transfer before turnover. For the ΔG121 mutants, this signal may be attributed either to a conformational change or to the binding of the second ligand. If the transient varies as a function of ligand concentration, then the resultant data were fit by a linear regression to yield the rate constants, k_{on} and k_{off}, for the ligand to bind and dissociate from the respective binary complex. Whenever the rate is independent of ligand concentration, the fluorescence transient was assigned to a conformational change. The observation of conformational changes or binding kinetics proved dependent on the nature of the binary complex and the mutations in the βF−βG loop.

For ΔG121 DHFR, the addition of H_2F to DHFR·NADPH results in a fluorescence transient occurring at a rate of 23 ± 1 s^{-1} with the ternary complex (Figure 2). The signal likely derives from a repositioning of the nicotinamide ring. This conformational change may occur before or after H_2F binds to DHFR·NADPH. In the first scenario, dihydrofolate binds to form an initial DHFR·NADPH·H_2F complex (I), which then isomerizes at the observed rate to yield the Michaelis complex from which reduction of H_2F occurs. Another possibility (II) is that the isomerization step occurs prior to H_2F binding with the latter serving as a kinetic trap driving the formation of the ternary complex. Due to the magnitude of the rate and the nature of the signal, the rate could not be unambiguously ascribed to an isomerization either before or after H_2F bound to the enzyme.

Upon reversing the order of addition, where cofactor is mixed with the DHFR·H_2F complex, two conformational changes are detected for ΔG121 DHFR. The fluorescence transients corresponding to these conformational changes are a rapid fluorescence increase (112 ± 11 s^{-1}), followed by a slower fluorescence decrease (5.9 ± 0.3 s^{-1}) prior to substrate turnover (Figure 3). As before, these signals likely reflect alterations in the environment of the nicotinamide ring of the cofactor. Unlike the ambiguity of the other fluorescent transient for ΔG121 DHFR, these conformational changes are positioned after NADPH binding for two reasons: (1) the observed signal requires NADPH to be already bound and (2) neither rate reflects NADPH binding.

For both 117.5G,ΔG121 and ΔG121,124.5G DHFRs, the position of the glycine insertion determined whether ligand binding or a conformational change was observed. For 117.5G,ΔG121 DHFR, the observed burst rate (k_b) increases from 20 to 100 μM NADPH (Figure 5). Fitting the resultant data to a simple association reaction (see Kinetics of Ligand Binding) yields the on and off rates of NADPH for the DHFR·H_2F complex (Table 5). Although k_{on} slightly decreases compared to wild type, k_{off} increases by 60-fold.

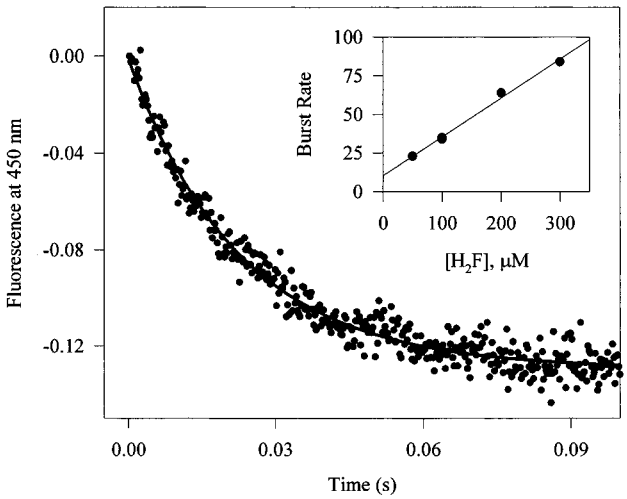

FIGURE 4: Substrate binding to DHFR·NADPH complex for glycine insertion mutant DHFRs. The larger graph is a representative curve of the fluorescence burst observed prior to steady-state turnover. Since the fluorescence transient occurs at a rate much greater than the steady-state rate, only the data for the fluorescence burst are shown and fit to a single exponential. The inset shows a linear fit of the burst rates versus substrate concentration. The corresponding binding constants are listed in Table 5. Reaction conditions were 3 μM DHFR, 100 μM NADPH, and varied H_2F at 25 °C in MTEN at pH 7.0.

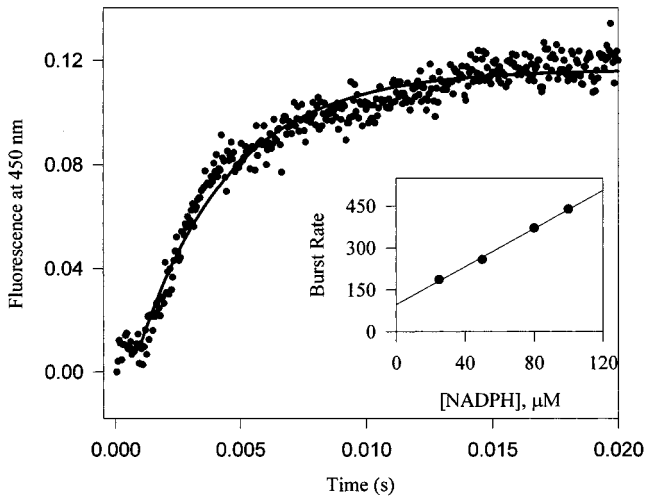

FIGURE 5: Cofactor binding to E·H_2F complex for 117.5G,ΔG121. The larger graph is a representative curve of the fluorescence burst observed prior to steady-state turnover. Since the fluorescence transient occurs at a rate much greater than the steady-state rate, only the data for the fluorescence burst are shown and fit to a single exponential. Attempts were made to fit the data to a double exponential. Although the rate for the first phase was similar to the value obtained by fitting the data to a single exponential, the rate for the second phase was inconsistent between samples derived from a low amplitude for this phase; thus only the data set for the first phase was used in the analysis. The inset shows a linear fit of the burst rates versus substrate concentration. The corresponding binding constants are listed in Table 5. Reaction conditions were 3 μM DHFR, varied NADPH, and 100 μM H_2F at 25 °C in MTEN at pH 7.0.

The affinity of NADPH for DHFR·H_2F decreases 140-fold as determined by k_{off}/k_{on}. The apoenzyme of this mutant exhibits a less dramatic decrease in cofactor binding, 7-fold versus 140-fold, indicating the binding of substrate is at the expense of cofactor binding to establish the Michaelis complex. In contrast, for wild type the affinity of NADPH for the apoenzyme and the enzyme−substrate complex are equivalent.

Unlike 117.5G,ΔG121 DHFR, the ΔG121,124.5G mutant displays two isomerizations of the ternary complex after NADPH binding to the DHFR·H_2F complex. These rates are both 4-fold higher than those of ΔG121 DHFR, occurring at 440 ± 9 s^{-1} for the fluorescence increase and 25 ± 2 s^{-1} for the fluorescence decrease (data not shown). These conformational changes may correspond to the same isomerization steps observed with the ΔG121 mutant to form the reactive complex.

For both 117.5G,ΔG121 and ΔG121,124.5G DHFRs, a conformational change associated with the binding of H_2F to DHFR·NADPH is absent. Rather, with these mutants, the measured fluorescence signal corresponds to substrate binding to the binary cofactor complex (Figure 4). The burst rate (k_b) increases from 50 μM to 300 μM H_2F and can be fit to a linear regression describing a simple association reaction (see Kinetics of Ligand Binding section). Compared to wild type, k_{on} for dihydrofolate to the binary complex is significantly lower, roughly 100-fold, whereas k_{off} is decreased moderately (Table 5). No effect on k_{off} is measured for ΔG121 DHFR (Table 2). When compared to wild type, the affinity of H_2F for the binary complexes of 117.5G,ΔG121 and ΔG121,124.5G DHFRs decreases 44- and 18-fold, respectively, as determined by k_{off}/k_{on}. The loss in the binding of dihydrofolate to the binary complex is also evident with the apoenzyme. Thus, the preincubation of mutant enzyme with NADPH does not reestablish important binding contacts present in wild type. Furthermore, the insertion mutants display a 2-fold difference in affinity of dihydrofolate binding favoring the apoenzyme, indicating a minor loss in binding interactions to form the ternary complex. For wild type a more pronounced 5-fold lower affinity of dihydrofolate for DHFR·NADPH versus DHFR alone is observed.

Summary of Overall Kinetic Scheme. By determining the kinetic rate constants for ligand binding and substrate conversion (Tables 2−4 and Figures 2 and 3), it is possible to construct a kinetic scheme for ΔG121 DHFR at pH 7.0 (Scheme 3). The complexity of its data set required a number of considerations to complete the scheme as shown. With regard to the formation of DHFR·NADPH·H_2F, the differences in the rates of the conformational changes

Table 5: Binding Kinetics Resulting in a DHFR·NADPH·H_2F Complex by ΔG121 Mutants and Wild-Type DHFRs

		wild type[a]			117.5G,ΔG121			ΔG121,124.5G		
ligand	enzyme species	k_{on} (μM^{-1} s^{-1})	k_{off} (s^{-1})	k_{off}/k_{on} (μM)	k_{on} (μM^{-1} s^{-1})	k_{off} (s^{-1})	k_{off}/k_{on} (μM)	k_{on} (μM^{-1} s^{-1})	k_{off} (s^{-1})	k_{off}/k_{on} (μM)
H_2F	DHFR·NADPH·H_2F	25 ± 8	40 ± 10	1.6 ± 0.5	0.25 ± 0.01	11 ± 1	44	0.26 ± 0.01	4.7 ± 2.2	19
NADPH	DHFR·NADPH·H_2F	5	1.7	0.3	2.9 ± 0.3	120 ± 20	41	ND[b]	ND	ND

[a] Taken from Fierke et al. (*8*). [b] ND, not determined.

Scheme 3: ΔG121 DHFR Kinetic Scheme at 25 °C in MTEN at pH 7.0[a]

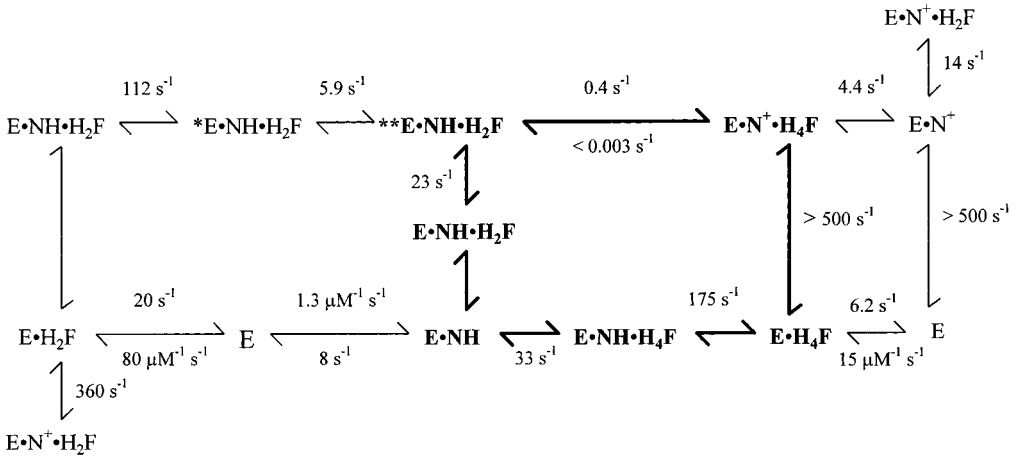

[a] NH = NADPH; N^+ = $NADP^+$; H_2F = dihydrofolate; H_4F = tetrahydrofolate.

between the initial binary complexes preclude equivalency of any of the intermediates; hence each path is treated independently in the full kinetic scheme. To simplify the scheme, only one of the potential paths is shown for the route leading to the ternary complex when DHFR·NADPH is the initial complex (Scheme 3). In the case of the reverse chemistry reaction, the detection limit of the assay provided a lower limit for this rate. The values of k_{on} for ligands to apoenzyme were calculated from k_{off} values and their respective K_D values by the relationship k_{off}/k_{on}. Although included in Table 3, the resulting off rates of cofactor and substrate from the ternary complex are not assigned in this scheme. The presence of multiple ternary complexes precludes the designation of the resulting binary complex upon release of ligand.

There are two striking features of the ΔG121 DHFR mechanism. First, deletion of Gly121 from the βF−βG loop affects all liganded complexes. The affinity for ligands, most notably for cofactor, decreases, as indicated by increased K_D values and off rates for ligands. Second, deletion of Gly121 dramatically affects the formation of the Michaelis complex (DHFR·NADPH·H_2F). Loss of this residue introduces novel conformational changes to attain the ternary complex upon addition of the second ligand to a binary complex. These conformational changes indicate multiple liganded enzyme forms are possible and that some are nonproductive. Furthermore, the Michaelis complex for ΔG121 DHFR proves to poorly coordinate ligands for chemistry, since the rate of hydride transfer is 550-fold lower than that observed for wild type. The nature of the effects of Gly121 deletion may underlie a dynamical, structural, or combined role for the βF−βG loop in DHFR catalysis.

Interestingly, substitution of Gly121 with valine results in similar effects on the DHFR catalytic cycle (*13*). This mutant retains wild-type binding for dihydrofolate and tetrahydrofolate; however, affinity for NADPH and $NADP^+$ decrease by 40- and 2-fold, respectively. The rate of hydride transfer by G121V DHFR indicates a 220-fold reduction in chemistry. This effect is significant enough to limit substrate turnover in the steady state. As observed from the deletion of Gly121, alteration of the βF−βG loop introduces a conformational change to the G121V DHFR catalytic cycle occurring at a rate of 3.5 s^{-1}. Taken together, these data are consistent with the crucial and potentially complex role the βF−βG loop plays in DHFR catalysis.

A goal of this study was to address the potential importance of Gly121 dynamical properties indicated in an NMR study of the binary folate complex (*7*). Indeed, deletion of this residue from the βF−βG loop results in the introduction of observable dynamical properties of the mutant enzyme. These transients occur on the millisecond time scale, corresponding to rates of 6 s^{-1}, 25 s^{-1}, and 110 s^{-1}. A slow exchange (33 s^{-1}) between Met20 conformations also occurs in the absence of ligand as demonstrated by an NMR study of apoenzyme (*6*). Moreover, slow exchange processes and ligand dynamics for the *Lactobacillus casei* DHFR suggest a similar conformational flexibility determining substrate specificity (*27*). The question remains as to whether this mutant alters a dynamic element of the wild-type catalytic cycle or are the observed conformational changes unique to this mutant. In the absence of further studies of this mutant, it is not possible to distinguish between these possibilities. Nevertheless, preliminary NMR data for the ΔG121 DHFR·folate complex do indicate attenutated backbone fluctuations for the βF−βG and Met20 loops (Peter Wright, personal communication).

A structural role for the βF−βG loop was elucidated in a recent publication of isomorphous X-ray crystal structures describing the liganded forms of DHFR in the catalytic cycle (*4*). In that study a striking observation is the presence of two ligand-dependent conformations of the Met20 loop, which seals the active site. A closed conformation occurs in the formation of DHFR·NADPH and the Michaelis complex (DHFR·NADPH·H_2F), and an occluded conformation, where the Met20 loop occupies part of the cofactor binding site, occurs in the DHFR·$NADP^+$·H_4F, DHFR·H_4F, and DHFR·NADPH·H_4F complexes. These Met20 loop conformations are stabilized by hydrogen bonds involving either the βF−βG loop in the closed conformation or the βG−βH loop in the occluded conformation. The preference of the Met20 loop conformations in either substrate or product complexes posits a functional role for Met20 loop flexibility.

Since the βF−βG loop does not directly contact ligands, the effects of the Gly121 deletion are transmitted through the Met20 loop. Deletion of Gly121 shortens the βF−βG

loop and may compromise the ability of the βF−βG loop to stabilize the closed Met20 loop conformation resulting in weakened substrate complexes. The deceased affinity for cofactor by ΔG121 DHFR is consistent with this conclusion. Furthermore, loss of the guiding influence of the βF−βG loop permits the flexible Met20 loop to sample alternate conformations. Conformational changes are observed for this mutant to attain the Michaelis complex and are similar in magnitude to the rate of exchange of the Met20 loop for apoenzyme (*6*). Reinsertion of glycine into the ΔG121 βF−βG loop generally eliminates these conformational changes, likely through reestablished contacts between the βF−βG and Met20 loops. Despite this renewed role for the βF−βG loop, the wild-type active site is not reconstituted by these modified βF−βG loops. Both insertion mutants display significant reductions in binding of NADPH and H_2F (>8-fold, Table 2) and in the rate of hydride transfer (>1000-fold, Table 3) compared to wild type. These effects underscore the critical role for the composition of the βF−βG loop to properly orient the Met20 loop for catalysis.

Concluding Remarks. Studies have attempted to link the apparent flexibility of the Met20 loop to a functional role in the DHFR catalytic cycle. X-ray crystallographic data implicate two Met20 loop conformations as key determinants of ligand specificity required in the DHFR catalytic cycle (*4*). On the other hand, NMR studies provide evidence for a dynamic exchange of the Met20 loop between two environments in apoenzyme (*6*). This loop exchange process occurs at a rate (33 s^{-1}) similar to the off rate of ligands, suggesting a gating motion may limit release of ligands. Here, we provide kinetic evidence from a mutant DHFR that illustrates the importance of interloop interactions to guide the conformational changes inherently possible with the Met20 loop. Deletion of Gly121 in the βF−βG loop reduces affinity for ligands, introduces novel conformational changes, and decreases significantly the rate of hydride transfer. All of these effects are transmitted through the Met20 loop. The outer βF−βG loop guides the formation of the appropriate Met20 loop conformations to modulate ligand specificity observed in the wild-type catalytic cycle and properly orient cofactor and substrate for efficient hydride transfer to occur. Since the DHFR catalytic cycle requires the modulation of ligand specificity, the role of βF−βG loop as a guide for complex formation is a dynamical process. Further analysis on the relationship of these interloop interactions and DHFR catalysis will prove enlightening.

ACKNOWLEDGMENT

We are very grateful to Dr. William Cannon for the preparation of Figure 1.

REFERENCES

1. Blakely, R. L. (1984) in *Folates and Pterins* (Blakely, R. L., and Benkovic, S. J., Eds.) pp 191−253, Wiley & Sons, Inc., New York.
2. Huennekens, F. M. (1994) *Adv. Enzyme Regul. 34*, 397−419.
3. Roth, B., and Stammers, D. K. (1992) in *The Design of Drugs to Macromolecular Targets* (Beddell, C. R., Ed.) pp 85−118, John Wiley & Sons Ltd., New York.
4. Sawaya, M. R., and Kraut, J. (1997) *Biochemistry 36*, 586−603.
5. Falzone, C. J., Benkovic, S. J., and Wright, P. E. (1990) *Biochemistry 29*, 9667−9677.
6. Falzone, C. J., Wright, P. E., and Benkovic, S. J. (1994) *Biochemistry 33*, 439−442.
7. Epstein, D. M., Benkovic, S. J., and Wright, P. E. (1995) *Biochemistry 34*, 11037−11048.
8. Fierke, C. A., Johnson, K. A., and Benkovic, S. J. (1987) *Biochemistry 26*, 4085−4092.
9. Cannon, W. R., Garrison, B. J., and Benkovic, S. J. (1997) *J. Am. Chem. Soc. 119*, 2386−2395.
10. Bystroff, C., and Kraut, J. (1991) *Biochemistry 30*, 7826−7833.
11. Gekko, K., Yamagami, K., Kunori, Y., Ichihara, S., Kodama, M., and Iwakura, M. (1993) *J. Biochem. (Tokyo) 113*, 74−80.
12. Gekko, K., Kunori, Y., Takeuchi, H., Ichihara, S., and Kodama, M. (1994) *J. Biochem. (Tokyo) 116*, 34−41.
13. Cameron, C., and Benkovic, S. J. (1998) *Biochemistry* (in press).
14. Sambrook, J., Fritsch, E. F., and Maniatis, T. (1989) *Molecular Cloning: A Laboratory Manual*, Cold Spring Harbor Laboratory Press, Cold Spring Harbor, NY.
15. Aiyar, A., Xiang, Y., and Leis, J. (1996) *Methods Mol. Biol. 57*, 177−191.
16. Williams, J. W., Morrison, J. F., and Duggleby, R. G. (1979) *Biochemistry 18*, 2567−2573.
17. Viola, R. E., Cook, P. F., and Cleland, W. W. (1979) *Anal. Biochem. 96*, 334−340.
18. Branlant, G., Eiler, B., and Biellmann, J. F. (1982) *Anal. Biochem. 125*, 264−268.
19. Blakely, R. L. (1960) *Nature (London) 188*, 231−232.
20. Mathews, C. K., and Huennekens, F. M. (1960) *J. Biol. Chem. 235*, 3304−3308.
21. Curthoys, H. P., Scott, J. M., and Rabinowitz, J. C. (1972) *J. Biol. Chem. 247*, 1959−1964.
22. Taira, K., and Benkovic, S. J. (1988) *J. Med. Chem. 31*, 129−137.
23. Velick, S. F. (1958) *J. Biol. Chem. 233*, 1455−1467.
24. Dunn, S. M. J., and King, R. W. (1980) *Biochemistry 19*, 766−773.
25. Cayley, P. J., Dunn, S. M. J., and King, R. W. (1981) *Biochemistry 20*, 874−879.
26. Birdsall, B., Burgen, A. S., and Roberts, G. C. K. (1980) *Biochemistry 19*, 3723−3731.
27. Roberts, G. C. K. (1991) *Host−Guest Molecular Interactions from Chemistry to Biology, Ciba Foundation Symposium 158*, p 169, Wiley, New York.

BI972922T